Basal-plane heat transport in graphite thin films

Yangyu Guo [1,2,3,*] Xiao-Ping Luo,[3] Zhongwei Zhang,[4] Samy Merabia,[1] Masahiro Nomura [2] and Sebastian Volz[2,5]

[1]*Institut Lumière Matière, Université Claude Bernard Lyon 1-CNRS, Université de Lyon, Villeurbanne 69622, France*
[2]*Institute of Industrial Science, The University of Tokyo, Tokyo 153-8505, Japan*
[3]*School of Energy Science and Engineering, Harbin Institute of Technology, Harbin 150001, China*
[4]*Center for Phononics and Thermal Energy Science, School of Physics Science and Engineering and China-EU Joint Lab for Nanophononics, Tongji University, Shanghai 200092, China*
[5]*LIMMS, CNRS-IIS UMI 2820, The University of Tokyo, Tokyo 153-8505, Japan*

While the phonon hydrodynamic regime has recently been highlighted experimentally in graphite films, the understanding and modeling of heat transport along their basal plane remain elusive. From first-principles-based modeling, we predict a significant influence of the surface roughness on basal-plane thermal conductivity due to the collective phonon drift. The occurrence condition of the phonon Knudsen minimum is also shown to strongly depend on the surface roughness. We summarize the basal-plane heat transport along graphite thin films into coherent and incoherent regimes and also present a speculation for the recently observed anomalous thickness-dependent thermal conductivity. Our work provides guidance for the experimental explorations of phonon hydrodynamics in graphitic micro- and nanostructures in the future.

I. INTRODUCTION

Understanding heat transport in graphite structures is important from both practical and fundamental points of view. Owing to its high basal-plane thermal conductivity (~ 2000 W/m K at room temperature), graphite has been applied as a thermal management material for heat dissipation in electronics [1–4]. The physics of phonon heat transport in graphite is peculiar due to the long-range van der Waals interaction along the out-of-plane c-axis direction [5] and its strong anisotropy [6]. The discovery of strong phonon hydrodynamic phenomena in graphitic materials in recent years [7–12] also highlights the significance of collective heat transport behaviors.

The theoretical modeling of the bulk thermal conductivity of graphite based on the phonon Boltzmann transport equation (BTE) has a long history. Early attempts are usually based on semiempirical phonon properties (dispersion and scattering rates) [13–16]. Recently, fully first-principles calculations have predicted the bulk experimental data [7]. In contrast, understanding the effect of finite thickness on the basal-plane heat transport along thin films of graphite remains inconclusive. A delicate experimental study [17] has shown that the thermal conductivity of multilayer graphene decreases and converges to that of bulk graphite as the number of atomic layers increases to ~ 5, which is consistent with the BTE modeling [18,19] based on a multilayer unit cell. However, another experiment [20] demonstrates a substantial decrease in the thermal conductivity of thin graphite with its thickness increasing from 8.5 to 580 μm, which contradicts the trend

in a recent work [21] combining theoretical and experimental investigations.

A few BTE models of the thickness effect on basal-plane heat transport use the phonon properties of bulk graphite. In a previous study [22], the classical isotropic Fuchs-Sondheimer (FS) model has been generalized to an anisotropic form based on the phonon BTE under the single mode relaxation time (SMRT) model, which predicted high basal-plane thermal conductivity even in graphite thin film with a thickness as small as 10 nm. However, the SMRT model has been shown recently to considerably underestimate the bulk basal-plane thermal conductivity of graphite due to strong phonon hydrodynamic behaviors [7,10,23]. The Monte Carlo (MC) solution of phonon BTE with an *ab initio* full scattering term [21] has led to the investigation of the thickness-dependent basal-plane thermal conductivity in the limit of fully diffuse thin film surfaces, while the effect of surface roughness is considered only for the case of one thickness corresponding to the experimental measurement.

In this work, we aim to conduct an extensive study on the effect of surface roughness on the thickness-dependent basal-plane heat transport along graphite thin films. A semianalytical solution of the phonon BTE under Callaway's dual relaxation model [24] is implemented, as a significantly more accurate approximation to the full scattering term than the SMRT model [23,25]. The present method is more efficient and provides a lower computational cost than that of a MC solution of phonon BTE with an *ab initio* full scattering term [21]. In addition, it provides straightforward insights owing to the semianalytical formulation and the intuitive physical interpretation. Our theoretical description also represents a more generalized formalism than the recent anisotropic FS model [22]. As a result, we reveal a significant thickness effect

---

*yangyuhguo@gmail.com
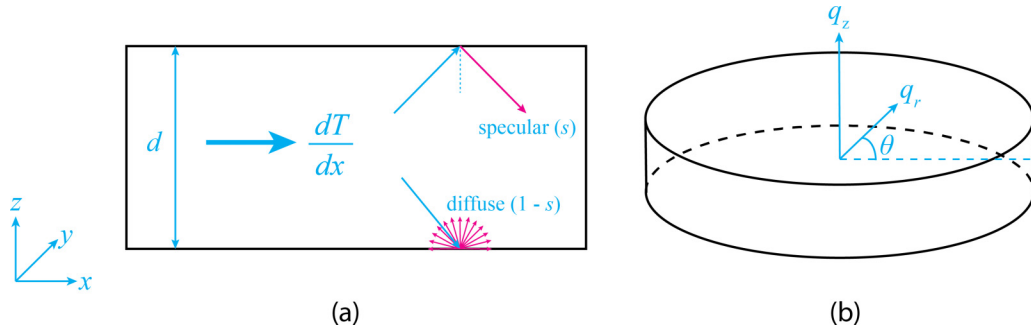
FIG. 1. Basal-plane phonon heat transport along a graphite thin film with a finite thickness d: (a) schematic of the physical model, where phonons experience partially specular and partially diffuse boundary scattering, with s referring to the specularity parameter; (b) approximate first Brillouin zone of graphite.

on the basal-plane thermal conductivity even in the presence of very smooth thin film surfaces. Furthermore, we investigate the effect of surface roughness on the phonon Knudsen minimum [10,26] in the thickness direction, as a hallmark of the transition from ballistic to hydrodynamic heat transport. This will enrich the knowledge of this peculiar phenomenon in graphitic materials, which was so far discussed only in the width direction and in the limit of fully diffuse surfaces [10,23,26,27].

The physical model and the mathematical methodology will be introduced in Sec. II. The results and discussion about the thickness and surface roughness effects on basal-plane heat transport are exposed in Sec. III, and Sec. IV will finally provide concluding remarks.

II. PHYSICAL AND MATHEMATICAL MODELS

In this section, the physical model of basal-plane heat transport along a graphite thin film with finite thickness is presented in Sec. II A. The phonon BTE under Callaway's dual relaxation time model and the corresponding boundary conditions are given in Sec. II B. In Secs. II C and II D, the semianalytical solution of the phonon BTE and model validation will be demonstrated.

A. Physical model

We model the steady-state heat transport along the basal plane of a graphite thin film with a finite thickness d and infinite length and width, under a uniform temperature gradient, as shown in Fig. 1(a). Only a finite thickness is investigated here, since the effects of finite length and/or finite width have been extensively studied [10,23,28]. Following our previous study [23], the hexagonal first Brillouin zone (BZ) is approximated as a cylinder with the basal-plane isotropy for simplified integration, as illustrated in Fig. 1(b). A semi-analytical solution of phonon BTE under Callaway's dual relaxation model is established following similar strategies to Refs. [10,27]. The partially diffuse and partially specular boundary condition is adopted at the surfaces of the graphite thin film, which is more general than that of previous studies [10,27] which use fully diffuse boundaries. In addition, the physical model is essentially different from those of the earlier studies, where heat transport in graphite ribbons [10]

and three-dimensional (3D) Debye crystals [27] with finite width were discussed, respectively. Note that the partially diffuse boundary condition was also adopted in the recent MC solution of phonon BTE with a full scattering term to study the temperature-dependent thermal conductivity of an ultrathin graphite film with a thickness of 23 layers [21].

B. Phonon Boltzmann equation and boundary condition

The phonon BTE under Callaway's dual relaxation model including the resistive and normal phonon scattering processes separately is written as [24,29]

$$\frac{\partial f}{\partial t} + \mathbf{v}_{\mathrm{g}} \cdot \nabla f = \frac{f_{\mathrm{R}}^{\mathrm{eq}} - f}{\tau_{\mathrm{R}}} + \frac{f_{\mathrm{N}}^{\mathrm{eq}} - f}{\tau_{\mathrm{N}}}, \tag{1}$$

where $f \equiv f(\mathbf{r}, t, \mathbf{q}, p)$ denotes the phonon distribution function, with $\mathbf{q}$, p, $\mathbf{v}_{\mathrm{g}}$ the phonon wave vector, polarization, and group velocity, respectively. The relaxation times of resistive and normal processes are denoted by τ_{R} and τ_{N}, with their equilibrium distribution functions defined separately as the Bose-Einstein distribution: $f_{\mathrm{R}}^{\mathrm{eq}} = \{\exp[\hbar\omega/(k_{\mathrm{B}}T)]-1\}^{-1}$ and the displaced one: $f_{\mathrm{N}}^{\mathrm{eq}} = \{\exp[(\hbar\omega-\hbar\mathbf{q}\cdot\mathbf{u})/(k_{\mathrm{B}}T)]-1\}^{-1}$, where $2\pi\hbar$ and k_{B} are the Planck and Boltzmann constants, respectively. The phonon drift velocity $\mathbf{u}$ is a macroscopic quantity, which is determined by the quasimomentum conservation condition of normal process [24]:

$$\sum_p \int \hbar\mathbf{q}\frac{f_{\mathrm{N}}^{\mathrm{eq}} - f}{\tau_{\mathrm{N}}}\frac{d\mathbf{q}}{(2\pi)^3} = 0. \tag{2}$$

The partially diffuse and partially specular boundary condition for the phonon BTE (1) is given as follows:

$$z = 0, \ f^{+}(0, \theta, q_r, q_z, p)|_{v_{gz}>0}$$
$$= (1-s)f_{\mathrm{R}}^{\mathrm{eq}} + sf^{-}(0, \theta, q_r, -q_z, p)\big|_{v_{gz}<0}$$
$$z = d, \ f^{-}(d, \theta, q_r, q_z, p)|_{v_{gz}<0}$$
$$= (1-s)f_{\mathrm{R}}^{\mathrm{eq}} + sf^{+}(d, \theta, q_r, -q_z, p)\big|_{v_{gz}>0}, \tag{3}$$

where s corresponds to the specularity parameter at the upper and lower surfaces of the graphite thin film. The present boundary condition includes the fully specular limit ($s = 1$) when the surface atomic planes are perfect [17] and the fully diffuse limit ($s = 0$) [10,22,27] when surface contaminations

are present [21]. The realistic surface specularity parameter depends on several factors, including the frequency and the incident angle of phonons, as well as the average height and the correlation length of the surface roughness [30,31]. The information on roughness can usually be extracted by AFM (atomic force microscopy) images of the surface [21]. An average constant value of the specularity parameter is assumed here as the first step of theoretical development and for the general discussion.

The deviational phonon distribution function is introduced [32]: $g = f - f_{\mathrm{R}}^{\mathrm{eq}}$, and a small deviation from equilibrium is assumed such that $f_{\mathrm{N}}^{\mathrm{eq}} \approx f_{\mathrm{R}}^{\mathrm{eq}} + T(\partial f_{\mathrm{R}}^{\mathrm{eq}}/\partial T)\mathbf{q} \cdot \mathbf{u}/\omega$ [24,26] and $\partial g/\partial x \ll \partial f_{\mathrm{R}}^{\mathrm{eq}}/\partial x$, $\partial f_{\mathrm{R}}^{\mathrm{eq}}/\partial z \ll \partial g/\partial z$. In this way, Eq. (1) is then reduced to

$$v_{gz}\frac{\partial g}{\partial z} + \frac{g}{\tau_{\mathrm{C}}} = \left[-v_{gx}\frac{\partial T}{\partial x} + \frac{T}{\tau_{\mathrm{N}}}\frac{q_x u_x}{\omega} \right]\frac{\partial f_{\mathrm{R}}^{\mathrm{eq}}}{\partial T}. \quad (4)$$

Equation (4) has the same form as the linearized phonon BTE for steady-state heat transport along graphite ribbon with a finite width [10]. The partially diffuse and partially specular boundary condition in Eq. (3) is simplified as follows:

$$z = 0, \; g^+(0, \theta, q_r, q_z, p)|_{v_{gz}>0} = s g^-(0, \theta, q_r, -q_z, p)|_{v_{gz}<0}$$

$$z = d, \; g^-(d, \theta, q_r, q_z, p)|_{v_{gz}<0} = s g^+(d, \theta, q_r, -q_z, p)|_{v_{gz}>0}. \quad (5)$$

C. Semianalytical solution

With the help of the boundary condition in Eq. (5), the solution of the deviational distribution function in Eq. (4) along the positive z direction is obtained as

$$g^+(\bar{z}, \theta, q_r, q_z, p)\big|_{v_{gz}>0}$$

$$= -\tau_{\mathrm{C}} v_{gx}\frac{\partial T}{\partial x}\frac{\partial f_{\mathrm{R}}^{\mathrm{eq}}}{\partial T}\left[1 + \frac{(s-1)e^{(-\bar{z}/Kn_{Cz})}}{1 - s e^{(-1/Kn_{Cz})}} \right]$$

$$+ \frac{1}{v_{gz}}\frac{\partial f_{\mathrm{R}}^{\mathrm{eq}}}{\partial T}\frac{Tq_x d}{\omega \tau_{\mathrm{N}}}\int_0^{\bar{z}} u_x(\bar{z}')\exp\left(\frac{\bar{z}'-\bar{z}}{Kn_{Cz}}\right)d\bar{z}'$$

$$+ \frac{1}{v_{gz}}\frac{\partial f_{\mathrm{R}}^{\mathrm{eq}}}{\partial T}\frac{Tq_x d}{\omega \tau_{\mathrm{N}}}\frac{s}{1 - s^2 e^{(-2/Kn_{Cz})}}\int_0^1 u_x(\bar{z}')$$

$$\times \left[s\exp\left(\frac{\bar{z}'-\bar{z}-2}{Kn_{Cz}}\right) + \exp\left(-\frac{\bar{z}'+\bar{z}}{Kn_{Cz}}\right) \right]d\bar{z}', \quad (6)$$

where we have introduced: $\bar{z} = z/d$ and the Knudsen number $Kn_{Cz} = v_{gz}\tau_{\mathrm{C}}/d$. The overall relaxation time is defined

by Matthiessen's rule as $1/\tau_{\mathrm{C}} = 1/\tau_{\mathrm{R}} + 1/\tau_{\mathrm{N}}$. The deviational distribution function solution along the negative z direction is

$$g^-(\bar{z}, \theta, q_r, q_z, p)\big|_{v_{gz}<0}$$

$$= -\tau_{\mathrm{C}} v_{gx}\frac{\partial T}{\partial x}\frac{\partial f_{\mathrm{R}}^{\mathrm{eq}}}{\partial T}\left[1 + \frac{(s-1)e^{[(1-\bar{z})/Kn_{Cz}]}}{1 - s e^{(1/Kn_{Cz})}} \right]$$

$$+ \frac{1}{v_{gz}}\frac{\partial f_{\mathrm{R}}^{\mathrm{eq}}}{\partial T}\frac{Tq_x d}{\omega \tau_{\mathrm{N}}}\int_1^{\bar{z}} u_x(\bar{z}')\exp\left(\frac{\bar{z}'-\bar{z}}{Kn_{Cz}}\right)d\bar{z}'$$

$$- \frac{1}{v_{gz}}\frac{\partial f_{\mathrm{R}}^{\mathrm{eq}}}{\partial T}\frac{Tq_x d}{\omega \tau_{\mathrm{N}}}\frac{s}{1 - s^2 e^{(2/Kn_{Cz})}}\int_0^1 u_x(\bar{z}')$$

$$\times \left[s\exp\left(\frac{\bar{z}'-\bar{z}+2}{Kn_{Cz}}\right) + \exp\left(-\frac{\bar{z}'+\bar{z}-2}{Kn_{Cz}}\right) \right]d\bar{z}'. \quad (7)$$

The deviational distribution function solution with $v_{gz} = 0$ is

$$g^0(\bar{z}, \theta, q_r, q_z, p)\big|_{v_{gz}=0} = -\tau_{\mathrm{C}} v_{gx}\frac{\partial T}{\partial x}\frac{\partial f_{\mathrm{R}}^{\mathrm{eq}}}{\partial T}$$

$$+ \tau_{\mathrm{C}}\frac{T}{\tau_{\mathrm{N}}}\frac{q_x u_x(\bar{z})}{\omega}\frac{\partial f_{\mathrm{R}}^{\mathrm{eq}}}{\partial T}. \quad (8)$$

The first terms on the right-hand side of Eqs. (6)–(8) are precisely the SMRT solution, and the other terms are relevant to the collective phonon drift. In the limit of fully diffuse ($s = 0$) surfaces, the semianalytical solution in Eqs. (6)–(8) will be reduced to an equivalent form to that given in Ref. [10] which accounts for the size effect from the finite width of the graphite ribbon, yet the present solution includes more general situations with finite specularity parameters.

The phonon drift velocity distribution in Eqs. (6)–(8) is determined with the help of the quasimomentum conservation condition in Eq. (2):

$$C_3 T u_x(\bar{z}) = F(\bar{z}) + \frac{\Delta q_z}{8\pi^2}\sum_p \sum_{q_z}{}_{v_{gz}>0}\int_0^{q_{r\max}}\frac{C_{\mathbf{q}p}q_r^3 d}{\omega^2 \tau_{\mathrm{N}}\Lambda_{\mathrm{N}z}}$$

$$\times \int_0^1 T u_x(\bar{z}')K(\bar{z}, \bar{z}')d\bar{z}'dq_r, \quad (9)$$

where the modal heat capacity is defined as $C_{\mathbf{q}p} = \hbar\omega\partial f_{\mathrm{R}}^{\mathrm{eq}}/\partial T$, and the first right-hand term and the integration kernel are, respectively,

$$F(\bar{z}) = -\frac{\partial T}{\partial x}\left(C_1 + \frac{\Delta q_z}{8\pi^2}\sum_p \sum_{q_z}{}_{v_{gz}>0}\int_0^{q_{r\max}}\frac{C_{\mathbf{q}p}q_r^2 \Lambda_{Cr}}{\omega \tau_{\mathrm{N}}}\left\{ 2 + \frac{s-1}{1 - e^{-1/Kn_{Cz}}}\left[\exp\left(-\frac{\bar{z}}{Kn_{Cz}}\right) + \exp\left(\frac{\bar{z}-1}{Kn_{Cz}}\right) \right] \right\}dq_r \right), \quad (10)$$

$$K(\bar{z}, \bar{z}') = \exp\left(-\frac{|\bar{z}'-\bar{z}|}{Kn_{Cz}}\right) + \frac{s^2}{1 - s^2 e^{(-2/Kn_{Cz})}}\left[\exp\left(\frac{\bar{z}'-\bar{z}-2}{Kn_{Cz}}\right) + \exp\left(\frac{\bar{z}-\bar{z}'-2}{Kn_{Cz}}\right) \right]$$

$$+ \frac{s}{1 - s^2 e^{(-2/Kn_{Cz})}}\left[\exp\left(-\frac{\bar{z}'+\bar{z}}{Kn_{Cz}}\right) + \exp\left(\frac{\bar{z}'+\bar{z}-2}{Kn_{Cz}}\right) \right]. \quad (11)$$
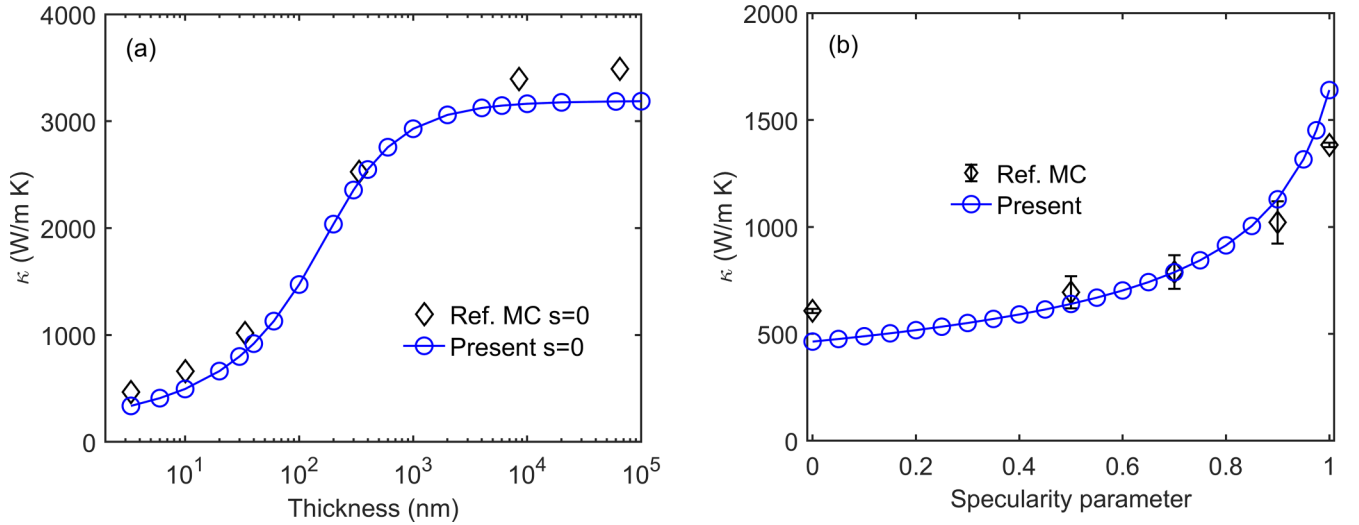
FIG. 2. Validation of the present model: (a) Thickness-dependent thermal conductivity at 200 K in the fully diffuse limit ($s = 0$). (b) Specularity parameter dependent thermal conductivity of a 23-layer graphite thin film at 300 K. The discrete diamond symbols with or without error bar represent the reference Monte Carlo (MC) solution of phonon BTE with *ab initio* full scattering term [21], whereas the solid line with circles denotes the present semianalytical solution of phonon BTE under Callaway's dual relaxation model.

where $\Lambda_{Cr} = v_{gr}\tau_C$, $\Lambda_{Nz} = v_{gz}\tau_N$, with $v_{gr} = \sqrt{v_{gx}^2 + v_{gy}^2}$. A rectangular numerical integration over q_z has been adopted with a uniform interval of Δq_z. Equation (9) is a Fredholm integral equation of the second kind, which is solved numerically with a Gauss-Legendre quadrature for the integration over $\bar{z}'$.

Once the solutions of the drift velocity and the deviational distribution function are derived, we obtain the heat flux distribution as $J_x(\bar{z}) = J_{x,\,\text{smrt}}(\bar{z}) + J_{x,\,c}(\bar{z})$, with the SMRT part and drift correction respectively:

$$J_{x,\,\text{smrt}}(\bar{z}) = -\frac{\partial T}{\partial x}\left(C_4 + \frac{\Delta q_z}{8\pi^2}\sum_p\sum_{q_z}\sum_{v_{gz}>0}\int_0^{q_{r\max}} C_{\mathbf{q}p} v_{gr}\Lambda_{Cr} q_r\left\{2 + \frac{s-1}{1-se^{-1/Kn_{Cz}}}\left[\exp\left(-\frac{\bar{z}}{Kn_{Cz}}\right) + \exp\left(\frac{\bar{z}-1}{Kn_{Cz}}\right)\right]\right\}dq_r\right),$$

(12)

$$J_{x,\,c}(\bar{z}) = C_1 T u_x(\bar{z}) + \frac{\Delta q_z}{8\pi^2}\sum_p\sum_{q_z}\sum_{v_{gz}>0}\int_0^{q_{r\max}}\frac{C_{\mathbf{q}p} v_{gr} q_r^2 d}{\omega\Lambda_{Nz}}\int_0^1 T u_x(\bar{z}')K(\bar{z},\bar{z}')d\bar{z}'dq_r.$$

(13)

In Eqs. (9)–(13), four constants $C_1 - C_4$ appear:

$$C_1 = \frac{\Delta q_z}{8\pi^2}\sum_p\sum_{q_z}\sum_{v_{gz}=0}\int_0^{q_{r\max}}\frac{C_{\mathbf{q}p} q_r^2 \Lambda_{Cr}}{\omega\tau_N}dq_r,$$ (14)

$$C_2 = \frac{\Delta q_z}{8\pi^2}\sum_p\sum_{q_z}\sum_{v_{gz}=0}\int_0^{q_{r\max}}\frac{C_{\mathbf{q}p} q_r^3 \tau_C}{\omega^2\tau_N^2}dq_r,$$ (15)

$$C_3 = \left(\mathbf{C}_{\tau_N}^1\right)_{xx} - C_2,$$ (16)

$$C_4 = \frac{\Delta q_z}{8\pi^2}\sum_p\sum_{q_z}\sum_{v_{gz}=0}\int_0^{q_{r\max}} C_{\mathbf{q}p} v_{gr}\Lambda_{Cr} q_r dq_r,$$ (17)

with the short notation in Eq. (16) defined as follows:

$$\mathbf{C}_{\tau_N}^1 = \sum_p\int\frac{C_{\mathbf{q}p}}{\omega^2}\frac{\mathbf{q}\mathbf{q}}{\tau_N(\mathbf{q},p,T)}\frac{d\mathbf{q}}{(2\pi)^3}.$$ (18)

Equation (12) is exactly the anisotropic FS model in the presence of a partially diffuse surface, and becomes equivalent to the model in Ref. [22] in the fully diffuse limit ($s = 0$). Equation (13) represents the drift correction from the

collective phonon transport, which plays a dominant role in graphite due to the strong hydrodynamic effect. The thermal conductivity of the graphite thin film is finally obtained by integrating the heat flux distribution along the thickness direction.

D. Model validation

Our semianalytical model requires the input of the phonon properties (dispersion relation and relaxation times) of bulk graphite. They are obtained from the fully first-principles calculation, with the details given in our previous study [23], where the phonon properties have been shown to accurately reproduce the bulk thermal conductivity of graphite. Note that here we adopt a $\mathbf{q}$ mesh of $40 \times 40 \times 7$ for the BZ discretization, with an odd number of discrete q_z to ensure the symmetry around the Γ point. In the following, the isotopically pure graphite is considered unless stated otherwise. We show the thickness-dependent thermal conductivity of graphite thin film in the fully diffuse limit ($s = 0$) at 200 K in Fig. 2(a). The result by the present Callaway

model is well consistent with that of the MC solution of phonon BTE with *ab initio* full scattering term [21]. The small difference is mainly due to a few reasons: (i) different scattering terms in BTE, i.e., the relaxation time model here versus the full scattering term [21]; (ii) different **q**-mesh discretizations, $40 \times 40 \times 7$ here versus $25 \times 25 \times 5$ [21]; (iii) slightly different results of first-principles calculation by different groups. To be specific, the slightly different thermal conductivities in the bulk limit should be dominated by reason (i); the difference in the small-thickness ballistic limit where the harmonic phonon bulk property (i.e., phonon dispersion) plays a decisive role shall be caused by both reasons (ii) and (iii); the better agreement in between is caused by the complicated interplay of all the reasons. In terms of the computational cost, the MC solution takes ~17 h using ten cores on a node ($2 \times$ AMD 7713, 128 cores, 256 GB memory) at the CADES cluster of the Oak Ridge National Laboratory for the simulation of a 65-μm-thick graphite film [21,33]. In contrast, the present semianalytical modeling of the same problem takes ~3 s using MATLAB R2020A on a laptop with an Intel i5-8265U processor (four cores). On the other hand, the phonon **q** mesh is relatively coarse in the MC solution of phonon BTE with the *ab initio* scattering term [21]. Those parameters indicate a much higher efficiency of the present model attributed to the Callaway's dual relaxation model appearing as an accurate approximation to the full scattering term of BTE. In addition, we show the specularity-parameter-dependent thermal conductivity of a 23-layer graphite thin film at 300 K in Fig. 2(b). The result by the present model generally agrees well with that by the MC solution of phonon BTE with the *ab initio* scattering term [21]. The noticeable difference in the fully specular limit ($s = 1$) comes from the fact that a finite length of 5 μm and a finite width of 1.75 μm are considered therein [21].

III. RESULTS AND DISCUSSION

In this section, first we will discuss the thickness and surface roughness effects on the basal-plane thermal conductivity of graphite thin film and the underlying mechanism in Sec. III A. In Sec. III B, the surface roughness effect on the phonon Knudsen minimum in the thickness direction will be investigated. Finally, some discussion and perspectives about the explanation of the experimental results and of future works are provided in Sec. III C.

A. Thickness and surface roughness effects on thermal conductivity

We conduct a detailed investigation of the thickness and surface effects on the thermal conductivity of graphite thin films at various temperatures. In Fig. 3(a), we consider graphite with natural abundance at 300 K and the fully diffuse limit to be the same as the conditions in Ref. [22]. The trend of the present SMRT solution is more or less consistent with that of the SMRT model in Ref. [22]. Some differences appear since the empirical phonon dispersion and relaxation times are adopted therein [22]. On the other hand, the present Callaway model shows appreciably smaller normalized thermal conductivity over the bulk value than that based on the SMRT
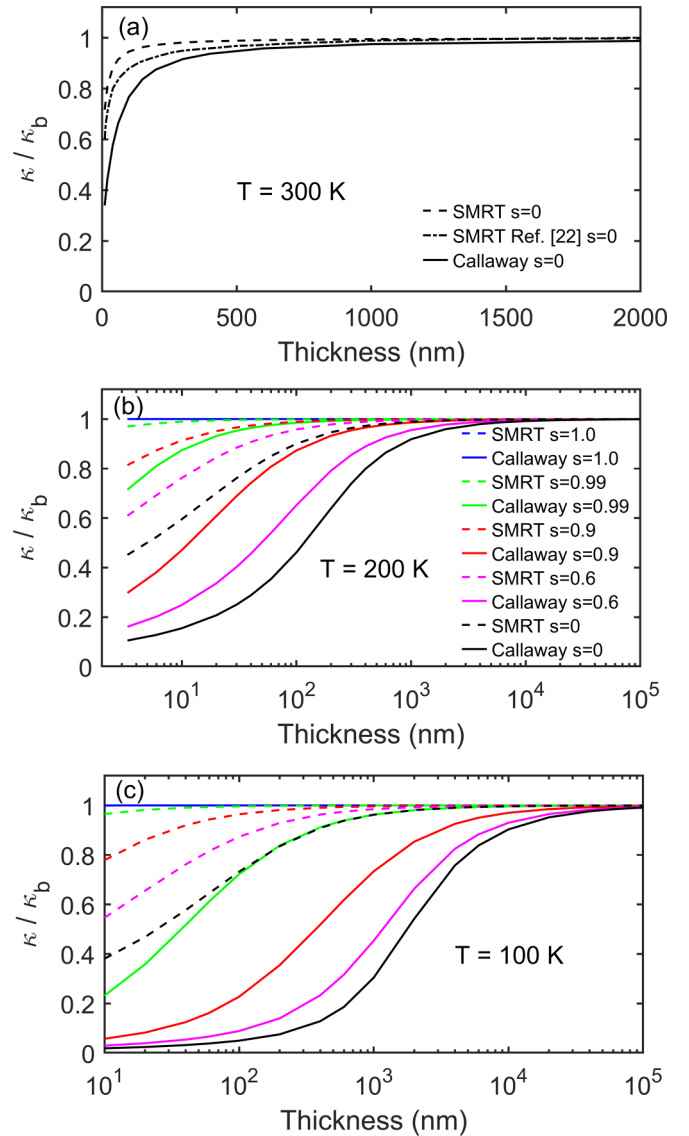
FIG. 3. Thickness-dependent normalized thermal conductivity of graphite thin film at different temperatures and various surface specularity parameters (s): (a) $T = 300$ K, natural graphite; (b) $T = 200$ K, isotopically pure graphite; (c) $T = 100$ K, isotopically pure graphite. The solid lines and dashed lines correspond to the present results based on phonon BTE under Callaway's dual relaxation model and under the single mode relaxation time (SMRT) model respectively. The dash-dotted line in (a) represents the reference SMRT model result [22]. In (a)–(c), $\kappa_b = 1.4724 \times 10^3$, 3.1891×10^3, and 1.6688×10^4 (W/m K), respectively, based on the present Callaway model, whereas $\kappa_b = 472.9132$, 628.0705, and 737.5010 (W/m K), respectively, based on the present SMRT model.

model. In other words, the present model predicts a stronger size effect from the finite thickness on the basal-plane heat transport. For instance, for a thickness of 10 nm, the Callaway model predicts ~70% reduction from the bulk value at 300 K whereas the SMRT model predicts only ~30% reduction of the thermal conductivity. The difference between the present model and the SMRT model turns out to be even larger at lower temperatures, as shown in Fig. 3(b) at 200 K and in Fig. 3(c) at 100 K for the isotopically pure graphite. Although
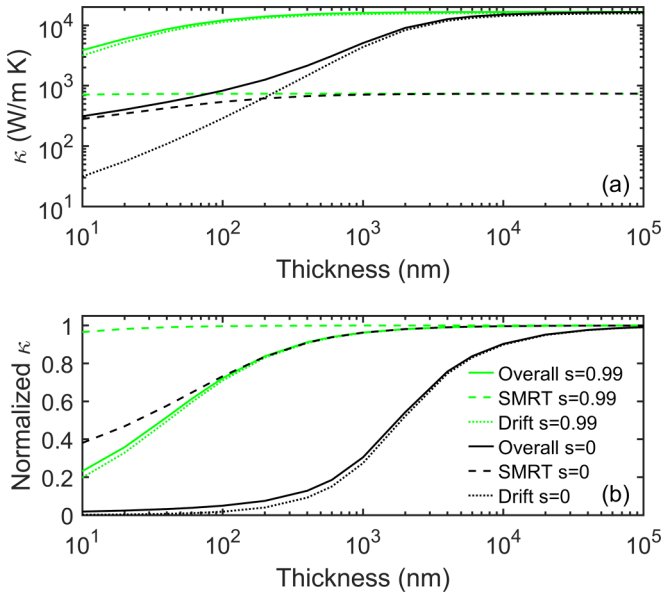
FIG. 4. Thermal conductivity decomposition in graphite thin film at 100 K: (a) thermal conductivity; (b) normalized thermal conductivity. The solid lines represent the overall result based on the phonon BTE under Callaway's dual relaxation model, whereas the dashed lines and dotted lines represent the single mode relaxation time (SMRT) part and drift correction. The normalization in (b) is done over the corresponding part in the bulk limit.

FIG. 5. Basal-plane phonon drift velocity distribution along the thickness direction in graphite thin film at 100 K and various surface specularity parameters (s): (a) thickness $d = 100$ nm; (b) thickness $d = 2$ μm. A temperature gradient of -1×10^8 K/m is implemented.

the SMRT model has been shown to significantly underestimate the bulk thermal conductivity of graphitic materials [7,8,23,25], its performance in the prediction of size effect in micro- and nanostructures has rarely been evaluated.

As the surface roughness is reduced and the specularity parameter s increases from 0 to 1, the size effect from the finite thickness of the graphite thin film generally weakens and finally vanishes, as shown in Figs. 3(b) and 3(c). In addition, we show an unexpected significant impact from the surface roughness on the basal-plane thermal conductivity. A very small deviation from the fully specular limit ($s = 1$) will induce a strong thickness effect on the thermal conductivity, as predicted by the Callaway model at $s = 0.99$ in Fig. 3(c) at 100 K. As the temperature increases to 200 K, the thickness effect at $s = 0.99$ becomes weaker but still non-negligible, as shown in Fig. 3(b). In both cases, the SMRT model predicts a negligible size effect as usually expected. It indicates that even tiny imperfections at the surface of a graphite thin film would remarkably deteriorate its basal-plane thermal conductivity.

To understand the physical mechanism behind this reduction, we report the decomposition of the overall thermal conductivity at 100 K into the SMRT part by Eq. (12) and the drift correction by Eq. (13) in Fig. 4(a). In the bulk limit (infinite thickness), the drift correction contributes to ∼95% of the overall thermal conductivity due to the strong hydrodynamic effect. In the case of a fully diffuse ($s = 0$) surface, the drift correction still has a predominant contribution at large thickness and decreases by more than two orders of magnitude at small thickness, where the SMRT part turns out to be dominant. In the case of a close to fully specular ($s = 0.99$) surface, the SMRT part is almost independent of the thickness,
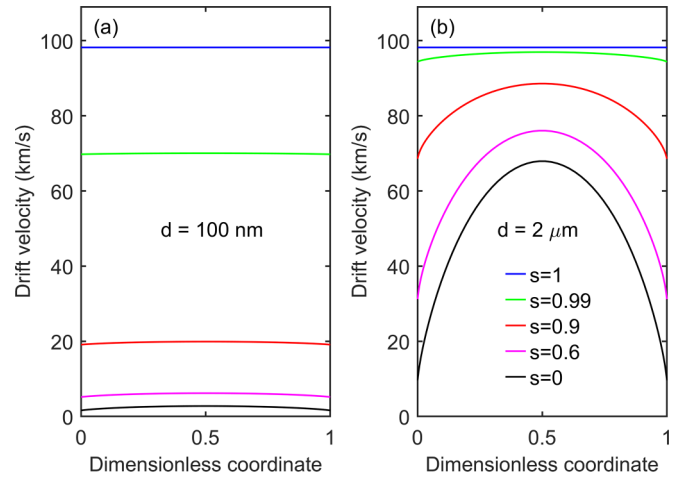
while the drift correction keeps dominant and decreases with a similar trend as that of the overall thermal conductivity with the thickness decreasing down to 10 nm. In all, the size effect from the finite thickness on the overall thermal conductivity is mainly governed by the drift correction, as clearly shown by their close normalized values over the corresponding bulk limit in Fig. 4(b). Therefore, the significant thickness and surface effects on the basal-plane heat transport in graphite thin film result from the strong impact of the boundary on the collective drift behaviors of phonons inside the structure.

For a straightforward picture of the impact of the surface on the phonon drift inside the graphite thin film, we display the drift velocity distributions in two structures at 100 K and various surface specularity parameters in Fig. 5. Based on the results of phonon mean free paths (MFPs) of normal and umklapp processes in recent studies [21,34,35], heat transport in the thin film with a thickness of 100 nm and 2 μm lies in the boundary scattering dominated regime and hydrodynamic regime respectively. In the case of 2 μm thickness, with decreasing specularity parameter, i.e., increasing surface roughness or imperfections, the phonon drift velocity is considerably reduced near the boundary, and is gradually transferred into the center of the thin film through normal phonon-phonon scattering processes. As the quasimomentum is conserved during normal processes, the impact from the surface on the phonon dynamics is much more efficiently transferred into the interior compared to that in the usual ballistic-diffusive regime [36,37]. In the latter case, the momentum-destroying resistive process is dominant, and the transfer of the surface impact is more easily interrupted and randomized. This analysis provides a microscopic picture for the much stronger thickness and surface effects predicted by the present model. In the case of 100 nm thickness, the phonon drift velocity distribution is more uniformly reduced due to frequent phonon-boundary scattering, and is much smaller compared to that of the 2 μm case at the same value of the specularity parameter ($s < 1$). In the close to fully specular ($s = 0.99$) surface, the reduction of drift velocity is still
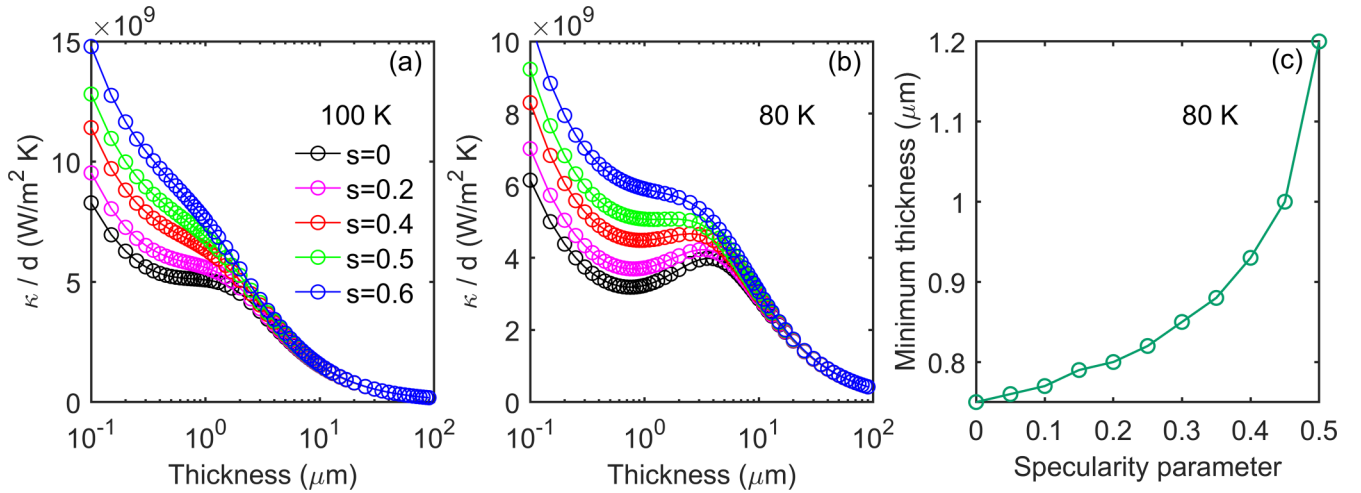
FIG. 6. Basal-plane thermal conductivity normalized by the film thickness (d) at different temperatures and various surface specularity parameters (s): (a) $T = 100$ K, (b) $T = 80$ K. (c) The thickness corresponding to Knudsen minimum as a function of surface specularity parameter at 80 K.

$\sim$30%, which provides a good explanation of the appreciable size effect shown in Fig. 3(c). Note that in the partially specular case, there are still normal and resistive processes after long-term boundary scattering processes. In fact, the effective thickness increases with increasing specularity parameter and becomes infinite in the limit of fully specular surface.

B. Surface roughness effect on phonon Knudsen minimum

In this subsection, we will explore the phonon Knudsen minimum in the thickness direction of graphite thin film and discuss the influence of surface roughness. The phonon Knudsen minimum delimits the transition from ballistic to hydrodynamic heat transport, which can be distinguished by the different size-scaling behaviors of the thermal conductivity [10,26]. The thermal conductivity increases linearly with the characteristic size and with the square of the characteristic size in ballistic and hydrodynamic regimes respectively [38,39]. Figure 6(a) shows the thermal conductivity normalized by the thickness of graphite film with various surface specularity parameters at 100 K. It is found that the normalized thermal conductivity always decreases monotonously with the film thickness. In other words, we do not obtain superlinear behavior of thermal conductivity, i.e., a phonon Knudsen minimum in the thickness direction at 100 K. For all surface specularity parameters, the normalized thermal conductivity has almost the same size-scaling behavior at smaller thickness ($d <\sim 300$ nm) where ballistic transport dominates. In the other limit, the normalized thermal conductivity converges to its bulk value at large thickness ($d >\sim 10$ μm). In between (~ 300 nm $< d <\sim 10$ μm), the decreasing slope of the normalized thermal conductivity increases as the specularity parameter increases.

We further lower the temperature down to 80 K where the phonon Knudsen minimum emerges, as shown in Fig. 6(b). The normalized thermal conductivity in the fully diffuse limit ($s = 0$) increases with film thickness after a Knudsen minimum at $\sim$750 nm and reaches a Knudsen maximum at $\sim$3.5 μm before decreasing again. As the specularity pa-

rameter increases, the phonon Knudsen minimum becomes weakened and disappears after $s > 0.5$. The underlying mechanism is the same as that for the aforementioned decreasing slope of normalized thermal conductivity in this intermediate thickness range. In this range, the thickness is larger than the intrinsic MFP of normal scattering processes whereas it is smaller than that of umklapp ones [21,34,35]. However, as the specularity parameter increases, phonons experience more specular surface scatterings which preserve the memory of their dynamics. Thus phonons have a higher probability to be involved in umklapp scattering after traveling an accumulated distance comparable to its intrinsic MFP before the memory-destroying diffuse surface scattering occurs. From another point of view, the effective thickness of the graphite thin film will increase to make space for the umklapp scattering when the surface specularity parameter increases, as discussed at the end of Sec. III A. This point can be quantitatively understood from the empirical expression of boundary scattering rate [40]: $1/\tau_b = [(1-s)/(1+s)]2|v_{gz}|/d$, which yields an effective thickness of $d_{\text{eff}} = d(1+s)/(1-s)$. The probability of an umklapp scattering event is given by $[1 - \exp(-d_{\text{travel}}/\Lambda_U)]$, where the accumulated traveling distance $d_{\text{travel}} \approx d_{\text{eff}}$. The boundary scattering rate can be refined based on the FS model, i.e., Eq. (12), and its qualitative trend will not change, as detailed in Ref. [40], and is not repeated here. As more umklapp scattering processes take place, the hydrodynamic behavior of phonons will be destroyed, and the phonon Knudsen minimum will gradually disappear. It indicates that sufficient roughness at the surface of graphite thin film is an essential ingredient for the observation of Knudsen minimum phenomenon in the thickness direction. For the phonon Knudsen minimum in the width direction of the graphite ribbon shown in previous works [10,23], a fully diffuse boundary is usually assumed since the edge of the graphite ribbon is roughened due to the etching method for patterning the ribbon in realistic experiment [34]. In contrast, special care should be paid to the surface roughness or imperfections in future experimental detection of phonon Knudsen minimum in the thickness direction of graphite. The surface specularity in the thickness
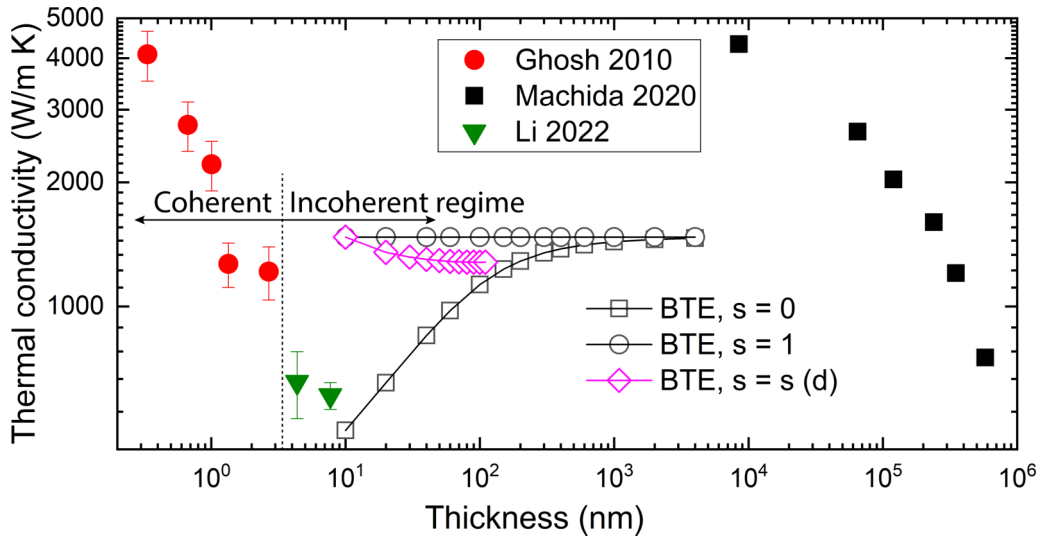
FIG. 7. Thickness-dependent thermal conductivity of graphite thin film along basal-plane direction around room temperature. The filled red circles denote the experimental data of multilayer graphene [17], the filled blacks squares denote the experimental data of graphite thin film at 250 K [20], and the filled green triangles denote the experimental data of $5.0 \, \mu m \times 3.4 \, \mu m \times 13$ layers and $5.0 \, \mu m \times 3.7 \, \mu m \times 23$ layers graphite samples [21]. The hollow black squares and circles with lines denote the present BTE model with a constant surface specularity parameter $s = 0$ and $s = 1$, respectively. The hollow magenta diamonds with line denote the present BTE model with a specularity parameter (s) decreasing linearly from 1.0 to 0.5 as the thickness (d) increases from 10 to 110 nm [$s = s(d)$].

direction can vary from fully specular [17] to fully diffuse [21] depending on the quality of graphite flakes usually obtained via a mechanical exfoliation process [17,21,34].

Another interesting finding in Fig. 6(b) is that the surface roughness has appreciable impact on the film thickness corresponding to the phonon Knudsen minimum. The minimum thickness shifts from ~ 750 nm to $1.2 \, \mu m$ as the surface specularity parameter increases from 0 to 0.5, as illustrated in Fig. 6(c). The underlying reason for this trend can be understood as follows. The Knudsen minimum represents a balance between the rarefaction effect from the boundary scattering and the collective effect from the normal scattering [26]. More explicitly, the rarefaction effect increases as the channel size decreases due to larger boundary slip whereas the collective effect increases as the channel size increases due to larger flux of heat carriers [41]. As the surface becomes smoother, the rarefaction effect becomes stronger, and the minimum thickness of the thin film shifts to a larger value. These results provide helpful guidance for future experiments and also a potential approach to modulate phonon hydrodynamic transport by surface modification.

C. Discussion and perspective

We would like to discuss the experimental results of thickness effect on the basal-plane thermal conductivity of graphite. The transition from two-dimensional (2D) to three-dimensional (3D) heat transport in few-layer graphene in the experiment [17] lies in the phonon confinement regime [21], i.e., coherent regime. As the thickness increases, the interlayer coherent interaction of lattice waves gradually forms the eigenmodes of graphite, and the thermal conductivity decreases from the value of single-layer graphene to that of bulk graphite. The underlying physics is essentially different from the size effect in the incoherent or particle transport

regime considered here, where the phonon properties of bulk graphite are adopted as inputs of the BTE modeling. To have a quantitative estimation of the critical thickness below which the coherent wave effect becomes important, we calculate the thermal conductivity accumulation function versus phonon wavelength in the Appendix. As shown in Fig. 8 in the Appendix, the wavelengths of dominant phonons contributing to heat transport in graphite are less than ~ 2 nm at room temperature, which is close to the thickness of 4–8 atomic layers where the thermal conductivity converges to bulk [17], as summarized in the left-hand side of Fig. 7. In principle, the range of thicknesses in the other experiment [20] corresponds to phonon heat transport in the incoherent regime, as summarized in the right-hand side of Fig. 7. However, the observed decrease of thermal conductivity with increasing thickness [20] contradicts the trend predicted by the BTE model in
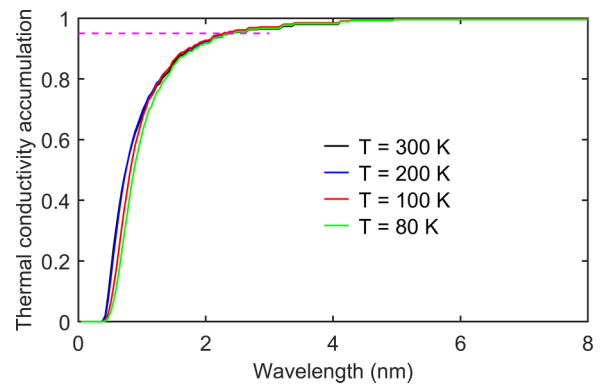
FIG. 8. Normalized thermal conductivity accumulation function versus phonon wavelength of bulk graphite along the basal-plane direction at different temperatures. The magenta dashed line denotes a 95% accumulation.

this work and in Refs. [21,22]. One possible reason for that anomalous trend is the worsening surface quality (decreasing specularity parameter) as the thickness increases, such that the surface effect prevails over the thickness effect. As an example, we presume that as the thickness increases from 10 to 110 nm the specularity parameter decreases linearly from 1.0 to 0.5, which produces even a decrease of thermal conductivity as shown in Fig. 7. Although the range of thicknesses in the experiment [20] is much larger, we intend to present one possible mechanism to explain the anomalous trend therein [20]. Finally, the experimental data of graphite thin films with 13 layers and 23 layers do not provide a clear conclusion about the thickness dependence [21]. There have been crucial experimental advances in investigating the thickness effect on heat transport along the c axis of graphite [42,43] inspired by previous theoretical modeling [44]. However, more experimental data are still needed in the future to have an unambiguous understanding of the thickness effect on the basal-plane heat transport of graphite.

Finally, note that the present semianalytical model only considers the effect of finite thickness, whereas realistic graphite structures have finite length and finite width as well [20,21,34]. To directly analyze future experimental data, we have to solve the phonon BTE in both the 3D reciprocal space and the 3D real space. In our recent work [23], we have developed a discrete-ordinates scheme to directly solve the phonon BTE under Callaway's dual relaxation model for heat transport in graphite ribbons with finite length and width. It is yet to generalize that numerical scheme to include the effect of finite thickness in the next step. In addition, a nature extension would be to account for the frequency-dependent specularity parameter.

IV. CONCLUSIONS

The thickness and surface roughness effects on the basal-plane heat transport in graphite thin film are investigated based on a semianalytical solution of the phonon Boltzmann equation under Callaway's dual relaxation model. We predict a significant effect of the surface roughness on the thickness-dependent thermal conductivity in the phonon hydrodynamic transport regime. The underlying mechanism comes from the strong impact of the surface on the collective phonon drift inside the structure due to the efficient quasimomentum transfer in normal phonon scattering processes. As the surface roughness is reduced, the phonon Knudsen minimum in the thickness direction is shown to weaken and the minimum thickness shifts to a larger value. The surface roughness provides a potential mechanism to qualitatively explain the recently observed anomalous trend of thickness-dependent thermal conductivity. Our theoretical prediction also gives useful guidance for future experimental detection of steady-state hydrodynamic heat flow in finite-sized graphitic materials.

APPENDIX: THERMAL CONDUCTIVITY ACCUMULATION FUNCTION VERSUS PHONON WAVELENGTH

Here we derive the thermal conductivity accumulation function versus phonon wavelength for bulk graphite based on the phonon BTE under Callaway's model [24]. Consider basal-plane heat transport along the x direction as shown in Fig. 1(a). The solution of the phonon BTE in Eq. (4) is reduced to

$$g = \tau_\mathrm{C}\left[-v_{\mathrm{g}x}\frac{\partial T}{\partial x} + \frac{T}{\tau_\mathrm{N}}\frac{q_x u_x}{\omega}\right]\frac{\partial f_\mathrm{R}^{\mathrm{eq}}}{\partial T}. \tag{A1}$$

With the help of the quasimomentum conservation condition in Eq. (2), we obtain the phonon drift velocity as follows:

$$Tu_x = -\beta\frac{\partial T}{\partial x}, \tag{A2}$$

where the factor between the drift velocity and temperature gradient is

$$\beta = \frac{\sum_p \int \frac{\tau_\mathrm{C}}{\tau_\mathrm{N}}\hbar q_x v_{\mathrm{g}x}\frac{\partial f_\mathrm{R}^{\mathrm{eq}}}{\partial T}\frac{d\mathbf{q}}{(2\pi)^3}}{\sum_p \int \frac{\tau_\mathrm{C}}{\tau_\mathrm{N}\tau_\mathrm{R}}\frac{\hbar q_x q_x}{\omega}\frac{\partial f_\mathrm{R}^{\mathrm{eq}}}{\partial T}\frac{d\mathbf{q}}{(2\pi)^3}}. \tag{A3}$$

Putting the solution in Eq. (A1) into the kinetic definition of heat flux, we get the expression of the thermal conductivity as

$$\kappa_{xx} = \sum_p \int \tau_\mathrm{C} v_{\mathrm{g}x} v_{\mathrm{g}x}\hbar\omega\frac{\partial f_\mathrm{R}^{\mathrm{eq}}}{\partial T}\frac{d\mathbf{q}}{(2\pi)^3}$$
$$+ \sum_p \int \frac{\tau_\mathrm{C}}{\tau_\mathrm{N}}\hbar q_x v_{\mathrm{g}x}\frac{\partial f_\mathrm{R}^{\mathrm{eq}}}{\partial T}\beta\frac{d\mathbf{q}}{(2\pi)^3}. \tag{A4}$$

The first term and second term in Eq. (A4) represent the SMRT part and drift correction, respectively. The thermal conductivity differential function versus phonon wavelength (λ) is defined as

$$\kappa_{\mathrm{diff}}(\lambda) = \sum_p \int \tau_\mathrm{C} v_{\mathrm{g}x} v_{\mathrm{g}x}\hbar\omega\frac{\partial f_\mathrm{R}^{\mathrm{eq}}}{\partial T}\delta\left(\lambda - \frac{2\pi}{|\mathbf{q}|}\right)\frac{d\mathbf{q}}{(2\pi)^3}$$
$$+ \sum_p \int \frac{\tau_\mathrm{C}}{\tau_\mathrm{N}}\hbar q_x v_{\mathrm{g}x}\frac{\partial f_\mathrm{R}^{\mathrm{eq}}}{\partial T}\beta\delta\left(\lambda - \frac{2\pi}{|\mathbf{q}|}\right)\frac{d\mathbf{q}}{(2\pi)^3}. \tag{A5}$$

The thermal conductivity accumulation function versus phonon wavelength is then calculated from the differential function as follows:

$$\kappa_{\mathrm{accum}}(\lambda) = \int_0^\lambda \kappa_{\mathrm{diff}}(\lambda')d\lambda'. \tag{A6}$$

As a result, the normalized thermal conductivity accumulation function with respect to the phonon wavelength in several temperatures of the current study are shown in Fig. 8.

[1] X. Luo, R. Chugh, B. C. Biller, Y. M. Hoi, and D. Chung, J. Electron. Mater. **31**, 535 (2002).

[2] A. Yu, P. Ramesh, M. E. Itkis, E. Bekyarova, and R. C. Haddon, J. Phys. Chem. C **111**, 7565 (2007).

[3] M. Inagaki, Y. Kaburagi, and Y. Hishiyama, Adv. Eng. Mater. **16**, 494 (2014).

[4] L. Li, A. Fukui, and A. Wakejima, Appl. Phys. Lett. **116**, 142105 (2020).

[5] E. Hazrati, G. A. de Wijs, and G. Brocks, Phys. Rev. B **90**, 155448 (2014).

[6] A. Minnich, Nanosc Microsc Therm Eng. **20**, 1 (2016).

[7] G. Fugallo, A. Cepellotti, L. Paulatto, M. Lazzeri, N. Marzari, and F. Mauri, Nano Lett. **14**, 6109 (2014).

[8] A. Cepellotti, G. Fugallo, L. Paulatto, M. Lazzeri, F. Mauri, and N. Marzari, Nat. Commun. **6**, 6400 (2015).

[9] S. Lee, D. Broido, K. Esfarjani, and G. Chen, Nat. Commun. **6**, 6290 6290 (2015).

[10] Z. Ding, J. Zhou, B. Song, V. Chiloyan, M. Li, T.-H. Liu, and G. Chen, Nano Lett. **18**, 638 (2018).

[11] S. Huberman, R. A. Duncan, K. Chen, B. Song, V. Chiloyan, Z. Ding, A. A. Maznev, G. Chen, and K. A. Nelson, Science **364**, 375 (2019).

[12] J. Jeong, X. Li, S. Lee, L. Shi, and Y. Wang, Phys. Rev. Lett. **127**, 085901 (2021).

[13] Y. A. Logatchov and A. S. Skal, Carbon **9**, 711 (1971).

[14] P. Klemens and D. Pedraza, Carbon **32**, 735 (1994).

[15] P. Klemens, J. Wide Bandgap Mater. **7**, 332 (2000).

[16] A. Alofi and G. P. Srivastava, Phys. Rev. B **87**, 115421 (2013).

[17] S. Ghosh, W. Bao, D. L. Nika, S. Subrina, E. P. Pokatilov, C. N. Lau, and A. A. Balandin, Nat. Mater. **9**, 555 (2010).

[18] L. Lindsay, D. A. Broido, and N. Mingo, Phys. Rev. B **83**, 235428 (2011).

[19] A. Alofi and G. Srivastava, Appl. Phys. Lett. **104**, 031903 (2014).

[20] Y. Machida, N. Matsumoto, T. Isono, and K. Behnia, Science **367**, 309 (2020).

[21] X. Li, H. Lee, E. Ou, S. Lee, and L. Shi, J. Appl. Phys. **131**, 075104 (2022).

[22] A. J. Minnich, Appl. Phys. Lett. **107**, 183106 (2015).

[23] Y. Guo, Z. Zhang, M. Bescond, S. Xiong, M. Wang, M. Nomura, and S. Volz, Phys. Rev. B **104**, 075450 (2021).

[24] J. Callaway, Phys. Rev. **113**, 1046 (1959).

[25] Z. Ding, J. Zhou, B. Song, M. Li, T.-H. Liu, and G. Chen, Phys. Rev. B **98**, 180302(R) (2018).

[26] Y. Guo and M. Wang, Phys. Rev. B **96**, 134312 (2017).

[27] X. Li and S. Lee, Phys. Rev. B **99**, 085202 (2019).

[28] X. Huang, Y. Guo, S. Volz, and M. Nomura, Appl. Phys. Express **15**, 105001 (2022).

[29] Y. Guo and M. Wang, Phys. Rep. **595**, 1 (2015).

[30] J. M. Ziman, *Electrons and Phonons: The Theory of Transport Phenomena in Solids* (Clarendon, Oxford, 1960).

[31] L. Maurer, Z. Aksamija, E. Ramayya, A. Davoody, and I. Knezevic, Appl. Phys. Lett. **106**, 133108 (2015).

[32] J.-P. M. Péraud and N. G. Hadjiconstantinou, Phys. Rev. B **84**, 205331 (2011).

[33] X. Li at Oak Ridge National Laboratory (private communication).

[34] X. Huang, Y. Guo, Y. Wu, S. Masubuchi, K. Watanabe, T. Taniguchi, Z. Zhang, S. Volz, T. Machida, and M. Nomura, Nat. Commun. **14**, 2044 (2023).

[35] Z. Ding, K. Chen, B. Song, J. Shin, A. A. Maznev, K. A. Nelson, and G. Chen, Nat. Commun. **13**, 285 (2022).

[36] G. Chen, Phys. Rev. Lett. **86**, 2297 (2001).

[37] M. Maldovan, Appl. Phys. Lett. **101**, 113110 (2012).

[38] R. Gurzhi, Sov. Phys. JETP **19**, 490 (1964).

[39] R. Gurzhi, Sov. Phys. Usp. **11**, 255 (1968).

[40] J. E. Turney, A. J. H. McGaughey, and C. H. Amon, J. Appl. Phys. **107**, 024317 (2010).

[41] G. Karniadakis, A. Beskok, and N. Aluru, *Microflows and Nanoflows: Fundamentals and Simulation* (Springer, New York, 2005).

[42] Q. Fu, J. Yang, Y. Chen, D. Li, and D. Xu, Appl. Phys. Lett. **106**, 031905 (2015).

[43] H. Zhang, X. Chen, Y.-D. Jho, and A. Minnich, Nano Lett. **16**, 1643 (2016).

[44] Z. Wei, J. Yang, W. Chen, K. Bi, D. Li, and Y. Chen, Appl. Phys. Lett. **104**, 081903 (2014).